

Failure Investigation of a 6th Stage Compressor Blade on a ETF40B Gas Turbine Engine

Gerrick Slogar (Gerrick.Slogar@Vericor.com)
Vericor Power Systems Inc.
3625 Brookside Parkway Suite 500
Alpharetta, GA 30022

Gary Prus (gprusla@comcast.net)
Parametric Solutions Inc.
900 East Indiantown Rd. Suite 200
Jupiter, FL 33477

Benjamin Canilang (benjamin.calilang@Navy.Mil)
Naval Surface Warfare Center, Carderock Division
Philadelphia, PA
Branch 935

1 Abstract:

Results from an engineering investigation, including findings, root cause and corrective action of a ETF40B compressor incident, are presented in this paper. Vericor's ETF40B is used to power US NAVY Landing Craft Air Cushion (LCAC) vehicles that have undergone the Service Life Extension Program (SLEP). This paper discusses the initial review of the failed engine, the results of the engineering investigation that led to identifying root cause and the successful validation testing providing fleet corrective action. This paper will present the history of the investigation, the metallurgical analysis findings, the finite element stress analysis results performed on the blade, the Fourier analysis performed on the bleed system and engine testing conducted to verify the investigation analysis. Additionally, this paper will discuss what caused the high stress levels in the blade along with the subsequent analysis conducted to define modifications to correct the problem. The paper will conclude with the testing conducted to verify the design solution and how the final field and production compressor changes were incorporated.

2 Introduction:

Vericor has been supplying the ETF40B to the US Navy since 2000 for its LCAC craft, as seen in Figure 1. Each craft has four engines, two mounted transversally on each side of the craft providing power for the lift fans and propulsion props. The ETF40B and is a replacement for the early TF40 engine first introduced in 1985 produces and 4745 Shaft Horse Power (SHP), a 14% increase from the TF40B at Navy standard day. Recently the US Navy experienced a high temperature shut down event on an ETF40B engine. Investigative disassembly revealed heavy compressor damage centered on the 6th stage compressor blade. Close examination of the 6th blade row found two (2) liberated blades at the root radius of the attachment. Both airfoil root attachments were intact and retained in the disk. The compressor showed heavy airfoil damage downstream of the 6th stage blade, but limited upstream damage.



Figure 1 Landing Craft Air Cushion (LCAC) Vehicle

3 Metallographic Investigation:

The fracture surfaces of the two missing 6th stage blades were visually and metallurgically interrogated to determine the failure mode and probable cause. The visual examination revealed a multiple origin transgranular fracture surface with no visible evidence of damage near the suspected origin, as seen in Figure 2. Stereomicroscopic review of the fracture surfaces revealed apparent origins near the pressure side and suction side mid-span area of both blade remnants. The pressure side origin was ~0.018” subsurface and the suction side origin appeared to be surface related, as seen in Figure 3. The fracture surface was predominantly transgranular, indicative of fatigue, with a small section of the fracture surface having an intergranular, dimpled appearance of the final overstress.

High magnification metallurgical examination was conducted to confirm and supplement the visual findings using Scanning Electron Microscopy (SEM). Both blade fracture surfaces were very similar in appearance and were predominately transgranular, which is typically indicative of fatigue propagation. Near the suction side trailing edges (and to a lesser degree, the pressure side leading edge area) a small area was observed that was intergranular and contained ductile dimple type overstress features. These intergranular areas were the final overstress regions when the airfoil separated from the two

sample attachment/platform/airfoil transition sections. High magnification SEM examination did reveal some striations contained in the transgranular areas. The striations are a reliable indicator of fatigue. After the fracture surface review in the scanning electron microscope, the sample 1 fracture was mounted, polished and etched to examine the cross sectional features.

The microstructure of Sample 1’s blade was examined for any anomalies and none were noted. The microstructure appeared typical for precipitation hardened AM350. Hardness readings were taken from Sample 1 and found typical of AM350 precipitation hardenable stainless steel in the heat treated condition – the average was HRC 41.

Fracture Surfaces Of Both Blades Are Similar, Uncommon Crack Initiation

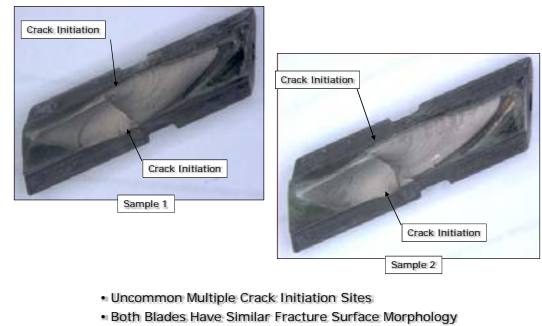


Figure 2 ETF40B 6th Stage Blade Fracture Surfaces

Subsurface Crack Initiation on Pressure Surface With Fatigue Propagation

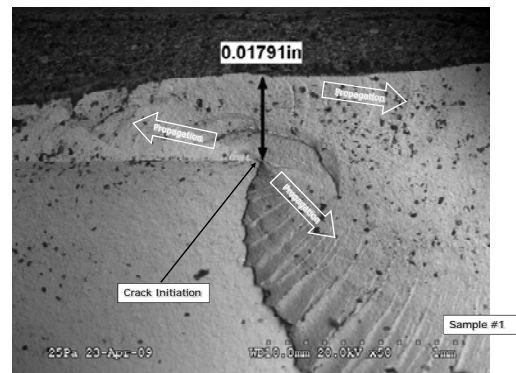


Figure 3 ETF40B 6th Stage Blade Fracture Surface Identifying Fracture Origin

Close examination of the root section from Sample 1's blade revealed the crack to propagate under the primary fracture surface, therefore the sample was broken open for close examination, as seen in Figure 4. Once the sample was broken open, it was apparent the primary crack propagated from the suction surface. There was a secondary crack initiation on the pressure surface. Both of the cracks propagated in opposite directions giving an appearance of a torsional failure mode. Based on the fracture surface and the multiple initiation sites, it can be concluded that the part saw high levels of fundamental cantilever bending mode stresses resulting in ultimate liberation of the airfoil.

Primary Crack Initiation on Suction Surface In Neck To Attachment Transition

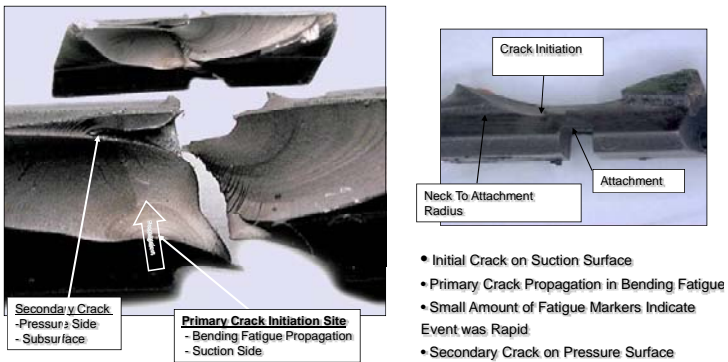


Figure 4 ETF40B 6th Stage Blade Fracture Surface Showing Multiple Origins

4 Analytical Investigation:

A detailed analytical investigation was initiated once the metallurgical investigation indicated a probable cause of the fracture. The purpose of this analysis was to corroborate the fracture mode. Three Dimensional (3-D) ANSYS Finite Element Analysis (FEA) was performed on the 6th stage blade to fully understand the operational stresses in the fracture area and to determine the most probable resonant mode that would produce the highest vibratory stress in the crack initiation

region. The 3D analysis included static stress prediction at operating conditions as well as resonance frequency predictions with normalized vibratory stress predictions.

The 6th stage blade model was finely meshed in the airfoil root attachment area to accurately predict static stresses. Once the ANSYS model was prepared and boundary conditions applied, the analysis was run at maximum operating conditions to determine the highest static loading in the part. The model results output were posted to allow for a fillet at the cross section of the primary crack location. The stress highest in the crack initiation area and can be seen in Figure 5

Modal stress predictions show the highest stress to be at the primary crack location for the 1st bending mode. All other predicted resonant mode stress did not generate high stresses in the primary fracture location. Therefore, the analysis corroborated the metallurgical findings indicating a high deflection simple bending mode fracture. The first bending or simple cantilever bending mode on the part produces similar vibratory stress on the suction and pressure surfaces, further corroborating the failure mode.

Analytical Modeling Predicts High Bending Modal Stresses at the Crack Initiation Site

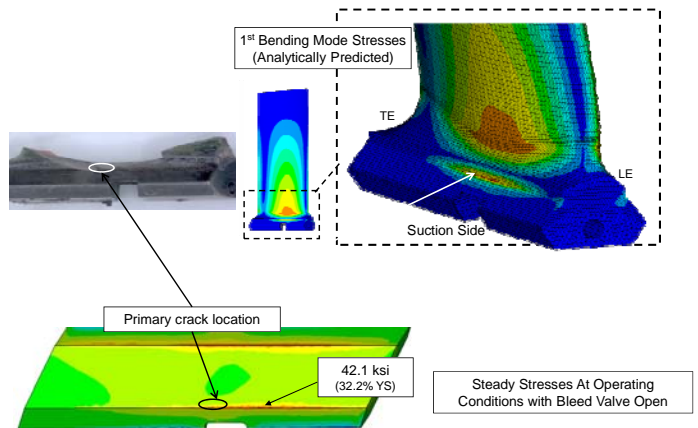


Figure 5 6th Stage Blade Structural Analysis Predictions of High Stresses in Crack Initiation Area

5 Investigative Engine Testing:

Instrumented investigative testing was completed in August 2009. Non-contacting Stress measurement System (NSMS) light probes were installed over the blade tips to measure each blade tip deflection during operation. The NSMS light probe array provides detailed tip deflection for each blade per revolution. The data recording system could determine the resonance speed for each individual airfoil. This was instrumental in understanding the frequency spread on the resonance of concern and if there were any low or high frequency anomalous blades.

High resonant stresses were observed on the 6th stage blade during normal operation of the engine. The stress on the 6th stage blade was determined to be driven by the compressor surge bleed system. The resonant crossing occurred at low power. No significant responses were noted on any part at high power throughout the test. A summary of the test results can be seen on the Campbell diagram in Figure 6. Figure 7 Summarizing the 6th Blade stresses on the Goodman diagram. This shows the measured stresses to be of concern.

This resonant response was determined to be the first bending mode driven by a 4 per revolution (4E) driver at approximately 16300 RPM. The maximum measured vibratory stress was normalized to be considered 100% of the maximum measured stress as seen in Figures 6 and 7. Figure 6 plots the resonance on the Campbell Diagram. This level of vibratory stress combined with the steady stress when plotted on a Goodman Diagram above the Goodman Limit, as seen in Figure 7. The 1st bending mode also showed a 6E response, with a lower stress measuring only 22% of the maximum measured stress at 9778 RPM. The significance of this resonant crossing is that it appears there is a strong 2 per rotor revolution (2E) driver in the engine

Figure 9 is an additional plot of the deflection on each of the 6th stage blades in a given revolution, the deflections are considered consistent from blade to blade and within expected results, with no anomalous blade response. The speed zone

of the resonance is also defined in this figure from 16128 to 16640. The variance in resonance speed is primarily driven by the geometric tolerances between each airfoil in the wheel. No high or abnormal resonances were observed at high speed/power, throughout the test.

This 1st bending 4E resonance is consistent with the failure investigation findings on the fractured 6th stage blades. The failure investigation sited the fracture mode was a 1st bending mode of high amplitude, therefore further test exploration of the resonance was performed that was not outlined in the original test plan.

Data reduction indicated that during a deceleration, the resonance would abnormally be excited as the engine transitioned from high speed through the speed zone of concern, as seen in Figure 8. It was determined this resonance change was related to the bleed valve opening on deceleration. It was concluded the bleed valve was the primary resonant driver. Therefore, further exploration of the resonance was conducted to determine if the resonance was driven by the exiting of bleed air from the bleed valve. This was completed by performing a normal start and forcing the bleed to be closed prior to the resonant speed zone of concern, 16128 to 16640 as illustrated in Figure 8. The 1st bending 4E resonant crossing occurred at the same speed zone, but the stresses were substantially reduced to a maximum observed stress of only 22% of the maximum stress observed with the bleed open. Plotting this stress level on the Goodman diagram shows the stress to be well within the Goodman allowable, as seen in Figures 6 through 9.

August 2009 Instrumented Test Identified Fracture Mode of 6th Blade

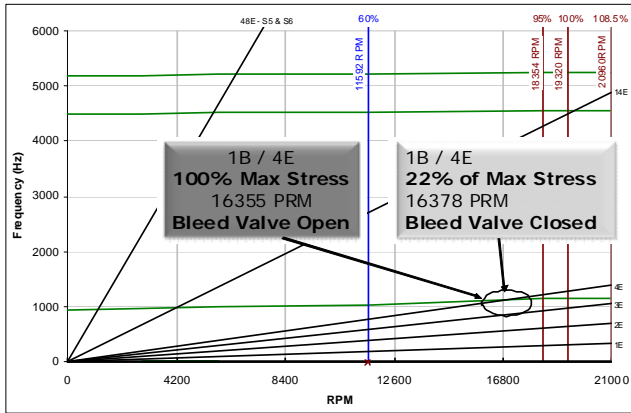
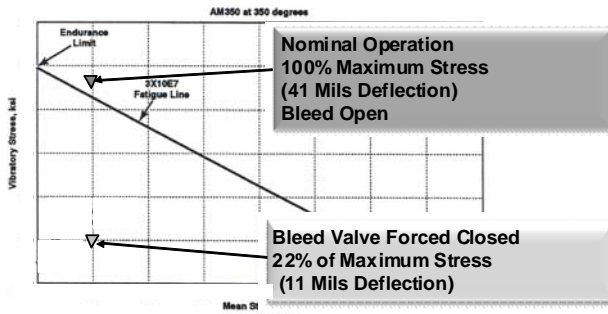


Figure 6 6th Stage Blade Campbell Diagram with Test Data

Instrumented Test Validated 6th Blade Stresses



• Structural Analysis Used for Mean Stress at the 4E Resonance Speed

Figure 7 6th Stage Blade Goodman Diagram

Bleed Valve Operation Is Directly Related to Stress Level

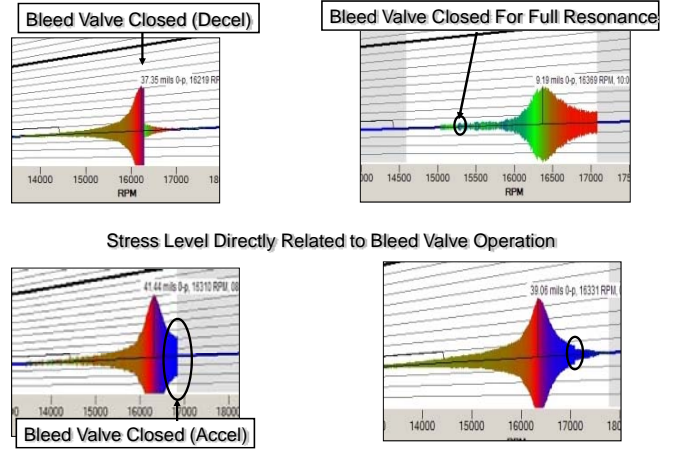


Figure 8 6th Stage Blade 1st Bending 4E Resonance Response with Bleed Open and Closed

ETF40B Strain Gage Results Show Resonance Speed Variation of 3.1%

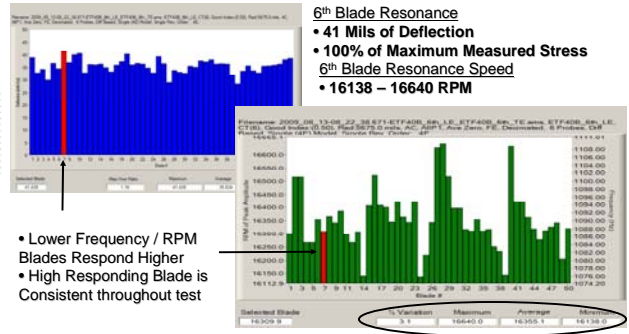


Figure 9 6th Stage 1st Bending 4E Individual Blade Deflections

6 4E Driver Analytical Investigation

Review of previous test data provided insight into the root cause of the 4E / 1st bending response driver. Historical 6th blade strain gage data taken during TF40 testing in the early 1970's showed a significant change of the 1st bending 4E response with the bleed open as compared to operation with the bleed valve closed. The data from the TF40 and ETF40B testing showed there was an impact to 6th blade stresses from the bleed system and the difference between the two

engine's bleed systems could account for the higher ETF40B stress levels. The ETF40B and TF40 bleed configurations can be seen in Figures 10 and 11. Figure 12 is a graphical depiction of the port size and quantity differences between the TF40B and the ETF40B. It can be seen that there are fewer and larger ports on the ETF40B. A comparison of the flow area for each of the bleed system components concluded the area at the flow path to be the same but elsewhere in the system showed significant differences in flow area and configuration. This can be seen in Figure 12. The flow area of the flow path consists of half circle cut outs forward edge between each vane and a gap between the forward edge of the stator and the compressor case. The 6th stator is attached to the compressor case by retention hooks, Figure 10, on the stator. The retention hooks are not in the same location for the TF40 and the ETF40B due to the configuration of the bleed slots. The hooks tend to separate the bleed flow into sections through each bleed slot.

A detailed Fourier analysis of the TF40 and ETF40B hardware configurations was generated to identify hardware configuration differences that would generate a 4E driver. The basic input parameters and methodology is seen in Figure 13. This analysis proved to be instrumental in understanding the 4E driver and ultimately reducing the 6th blade 4E 1st bending resonant stresses. The Fourier analysis evaluated the blockages in the bleed port, including the 6th vane attachment hook and half circles, bleed port size and location. Experimental engine data obtained from a previous test was not adequate to separate the effects of the 6th vane retention hook and the half circle cut outs in-between each airfoil; therefore the analysis included the effects of these features, as seen in Figure 10.

The initial results from the Fourier analysis of the TF40 compared to the ETF40B showed that the 4E driver was significantly stronger in the ETF40B as compared to the TF40, as seen in Figure 15. The results were interrogated to understand the 4E driving function in the ETF40B, or the lack of the 4E driver in the TF40. It was discovered that the TF40 bleed port design generated two 4E signals that are out of phase with each other, thus the two signals cancel each

other resulting in lower overall amplitude of the 4E driver in the TF40, as seen in Figure 14. The ETF40B configuration created a 4E and a 6E pattern with the 4E signal prediction being larger than the 6E, these results can be seen in Figure 14. Additionally, the ETF40B 4E and 6E configuration could potentially amplify each other as compared to the signal cancelation that occurs in the TF40.

To replicate the TF40 design philosophy of generating a signal that canceled or greatly reduced the baseline 4E ETF40B signal, a design study of multiple configurations was completed. Design ground rules were established to ensure the corrective action could be retrofitted into existing compressor cases and also be incorporated in the manufacture of a production case. The primary conceptual design was to modify the bleed port areas in the compressor case and allow for replication of the vane hooks and half moon blockage similar the TF40 design.

Two primary design concepts were selected out of numerous configurations for further consideration. The primary design generated a 4E response that was out of phase with the baseline compressor case 4E signal, which included additional blockage at the bleed exit port labeled MP2 to further reduce the 4E signal. This configuration was labeled Configuration 1. The second option considered, Configuration 2, was established to generate two separate 2E responses. This configuration provided a higher predicted 4E response, but greatly reduced the predicted 2E response from the baseline ETF40B. Based upon the strong 4E response and a weak 6E response observed during the exploratory testing.

Bleed plate blockers were fabricated for the Configuration 1, as identified above. The plates were designed and fabricated to allow for plate change out to without altering any engine hardware, other than the 7th stage stator retaining bolt, as seen in Figures 16.

ETF40B Bleed System Overview

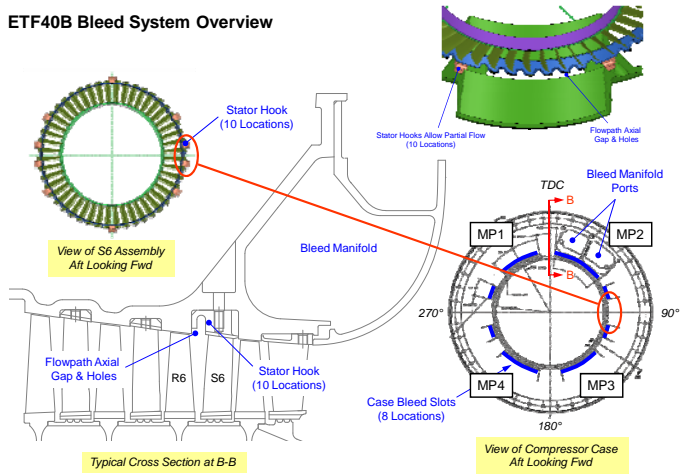


Figure 10 ETF40B 6th Stage Bleed Configuration

TF40 Bleed System Overview

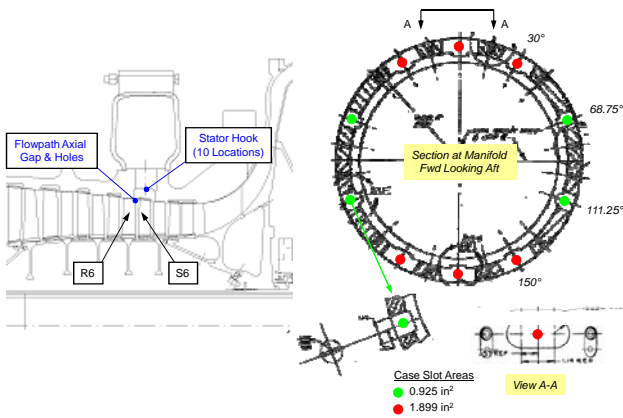


Figure 11 TF40 Bleed Configuration

TF40 / ETF40B Case Bleed Slot Flow Area Comparison

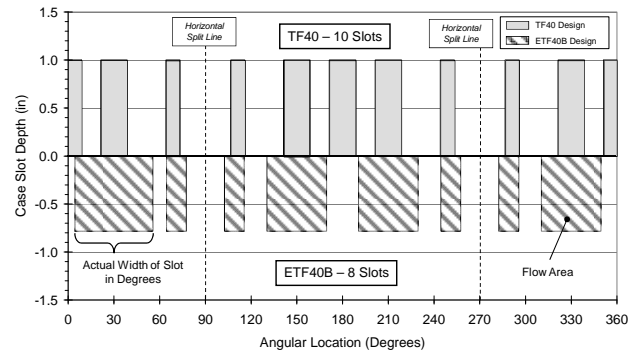
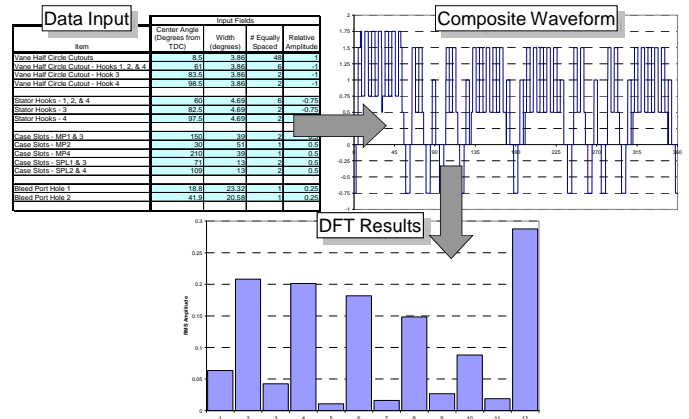


Figure 12 Compressor Case Bleed Port Comparisons between the ETF40B and the TF40

Data Input used to Construct Waveforms and Generate Predicted Fourier Results



F

Figure 13 Fourier Analysis Model

- Driver Pattern Comparison Between the TF40 and the ETF40B shows a Significant Pattern Difference in the Bleed Port Design
- TF40 Pattern Generates a Two Out of Phase 4E Patterns that Cancel Each other Out
- The ETF40B Generates a 6E Pattern

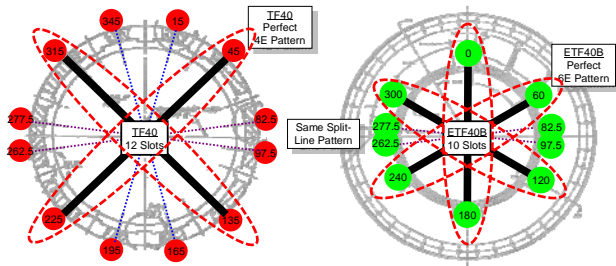


Figure 14 ETF40B and TF40 Configuration

ETF40B Fourier System Response Analysis

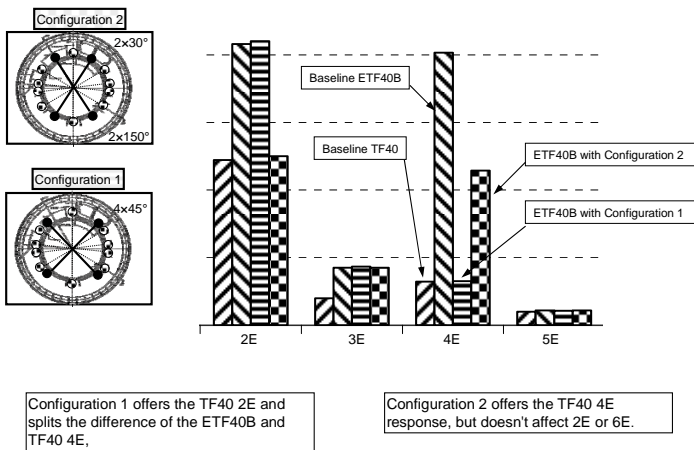


Figure 15 Fourier Analysis Results

Configuration 1 – (4E at 45 Degrees) With 50% Blocker at MP2

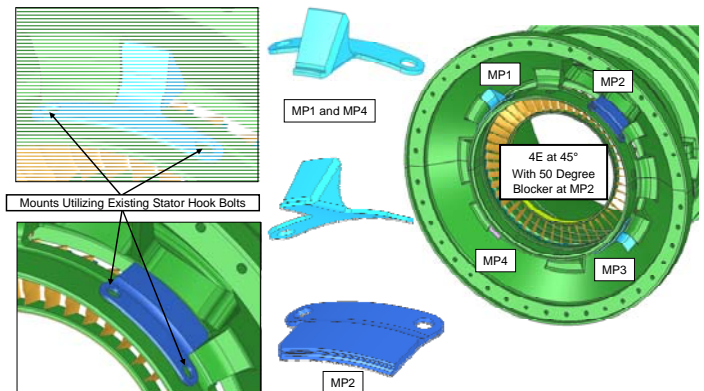


Figure 16 Final Blocker Plate Final Configuration (4 plates at 45 Degrees with 50% Blockage at MP2)

7 Validation Results

The 6th stage bleed plates were successful at modifying the 4E / 1st bending response, as seen in Figures 17 through 21. Non-Contacting Stress Measurement (NSMS) light probes were used to measure each blade tip deflection. The light probes were installed at the same location as in the original Investigation test outlined in Section 5. The data was recorded during testing, with and without the bleed open as well as during normal engine operation to ensure no responses were near the predetermined limits for each resonant mode.

The test plan was set to evaluate the configuration 1 blocker plates configuration, as identified in Figure 16. This was based upon the Fourier analysis and close integration of the investigative testing discussed in Section 5 above. Installation of the configuration 1 blocker plates that generated a 4E response similar to the TF40 with additional blockage at the MP2 location substantially reduced the 1st bending 4E response to 20% of the baseline configuration stress. The 6E response was very similar in amplitude to that of the baseline engine run.

The 5E 1st bending response increased slightly from the baseline testing, but was still below the 60% Goodman allowable limit. Historical investigation showed this stress level to be similar to operating stresses measured in the TF40 engine. These deflections are reported with the bleed open. This configuration proved to be the best overall solution at reducing the 6th blade stresses, as seen in Figures 17 through 21.

Converting the blade tip deflections to blade stresses was completed by employing the results from the ANSYS structural analysis. A correlation was made between tip deflection and stress at the 6th blade root in the 1st bending modal results. Once the relationship was established, all the tip deflections were converted into maximum stresses at the root location. The vibratory stress was then plotted with the predicted steady stress from the ANSYS structural model on a Goodman diagram, as seen in Figure 18. The 4E and 5E modal stress was plotted on this diagram. Both the 4E and the 5E stresses are well within the 60% Goodman capability. This Goodman Diagram also shows the substantial decrease in vibratory stress with the final configuration blocker plates for the 4E response.

6th blade stresses with the bleed closed were acceptable as seen in Figure 28 and Figure 20. The baseline tip deflections and stresses that were taken during the August 2009 test are considered acceptable. The stresses measured during this test further reduce the levels in every blocker plate configuration.

The 4E / 1st Bending response that was recorded during this test is the same response and driver of the response that was identified in the initial test in August 2009. Figure 21 contains the individual blade specifics for the speed of the resonance, the amplitude comparison between each blade, and the response with the bleed open and the bleed closed.

Blocker Plate Validation Test Results

Configuration	Bleed Open		
	1st Bending Response (Mils 0-Peak)		
	4E	5E	6E
Baseline (August 2009)	41.4	3.6	11.8
Configuration 1	8.3	21.4	17.7

Configuration	Bleed Open		
	1st Bending Response Stress as Compared to Maximum Measured		
	4E	5E	6E
Baseline (August 2009)	100%	9%	29%
Configuration 1	20%	52%	43%

Figure 17 6th Blade Test Results for the Final Configuration

Blocker Configuration Successfully Reduces Stresses to Acceptable Levels

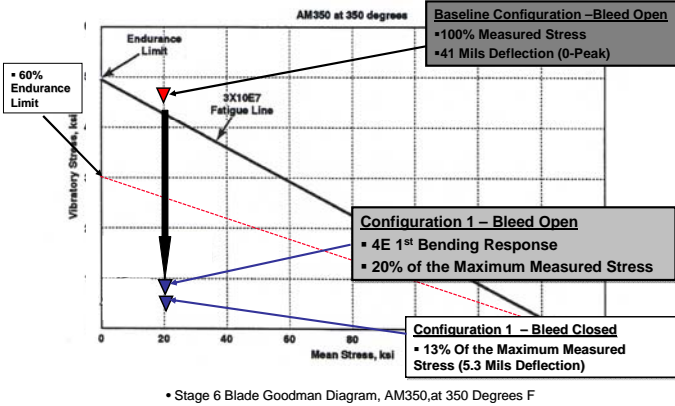
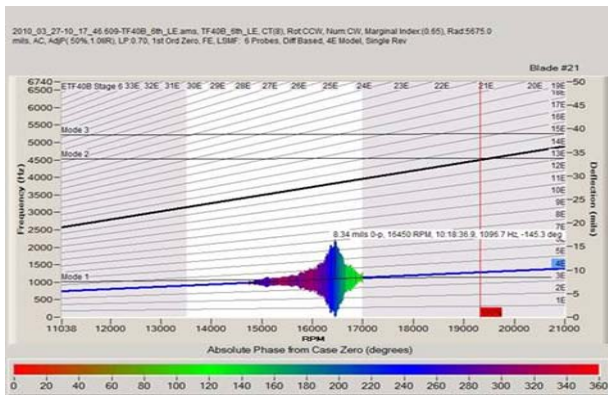


Figure 18 6th Blade Goodman Diagram Comparing the Baseline Stress to the Final Blocker Plate Configuration

4E 1st Bending Resonance Reduced to Low Levels



Characteristics of the Response Identical to Baseline Response Speed Region

Figure 19, 6th Blade Resonance with the Final Plate Configuration – Bleed Open

Bleed Valve Closure Further Reduces Response To Low Levels

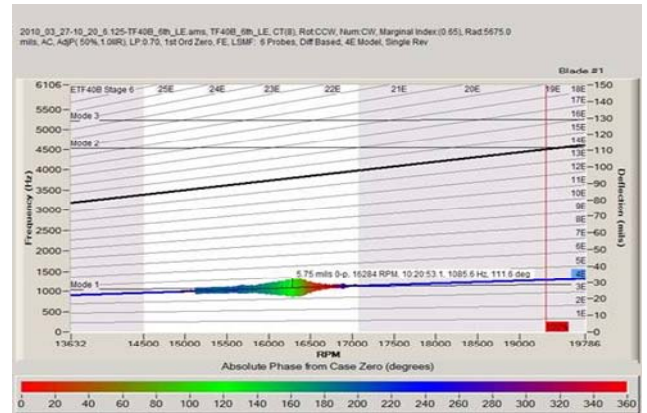


Figure 20, 6th Blade Resonance with the Final Plate Configuration – Bleed Closed

Resonance Characteristics (Speed and Frequency) Identical to Baseline With Reduced Deflection and Stress

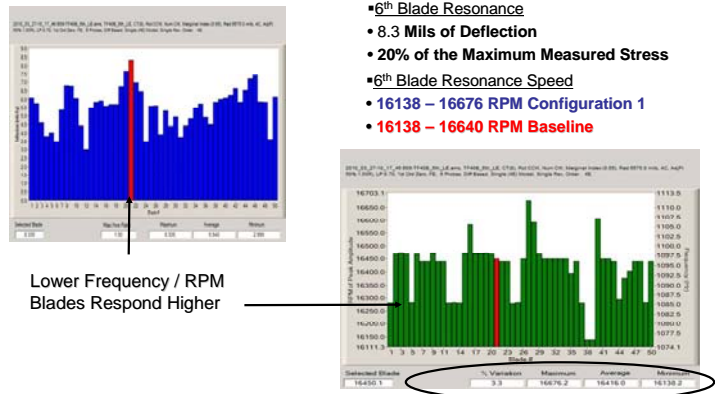


Figure 21, 6th Blade 1st Bending Response

8 Performance and Operability Evaluation of the Blocker Plates

The final blocker plate design, configuration 1 can be seen in Figures 22 and 23. The blades at the MP1, MP3 and MP4 locations were 7.5 degrees wide, while the blocker plate at the MP2 location provided 50% blockage of the flow area. The design used the 7th stage stator retention blot to retain the plate. Each plate used two of the 7th stator bolts to ensure full retention. The design incorporated a longer 7th stator bolt made from the

same material; a spacer was design to be plated under the plate to ensure the proper fit in the case. The plate stiffness design was optimized by incorporating relief cuts in the plate. This was incorporated to reduce the stresses in the retention bolt and plate. To ensure the plate did not induce wear issues with the case, a wear coating was applied to the contact surface between the plate and case. The design, showing installation into the case can be seen in Figure 23.

Adding the bleed blocker plates does not restrict the bleed flow area to a lower value than the flow path entrance at the 6th stator and thus did not affect the engine performance. This assumption was validated by back-to-back performance and operability engine testing. Validation testing was performed on a production engine, where baseline performance and operability characteristics were documented. The engine was then reconfigured with the blocker plates. The engine was re-installed in the test stand and the performance and operability testing duplicated. The results showed no discernable difference in the performance and operability of the engine during testing.

9 Fleet Modification

9.1 Fleet Retrofit Modification

Retrofit of the existing fleet started in September 2010. The retrofit process involved removal of all fielded engines, opening of the case, and installation of the blocker plates. Per the design concept, longer 7th stage stator bolts and spacers retained each plate in its proper position. Additionally each plate incorporated the anti-gallant coating on the plate-to-case contact surfaces. The final configuration resulting in the installation of four (4) plates at 45 degrees with the MP2 port blocked by 50% to match the configuration shown in Figures 22 and 23.

The long term solution will incorporate these bleed modifications into the compressor case itself during manufacture, modifying the bleed flow area removing the need to install the blocker plates.

Field Retrofit Blocker Plate Configuration

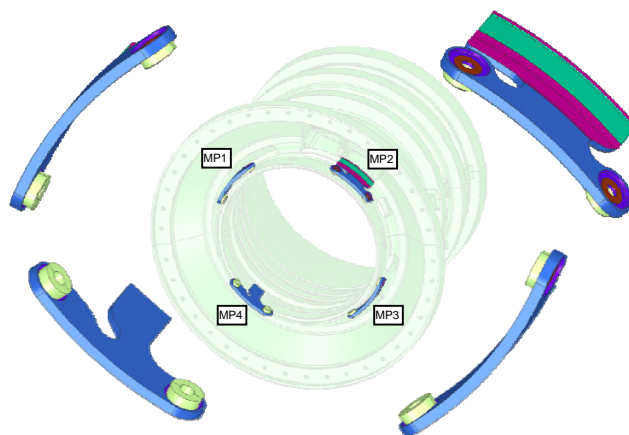


Figure 22, 6th Bleed Field Retrofit Configuration

Field Retrofit Blocker Plate Cross Section

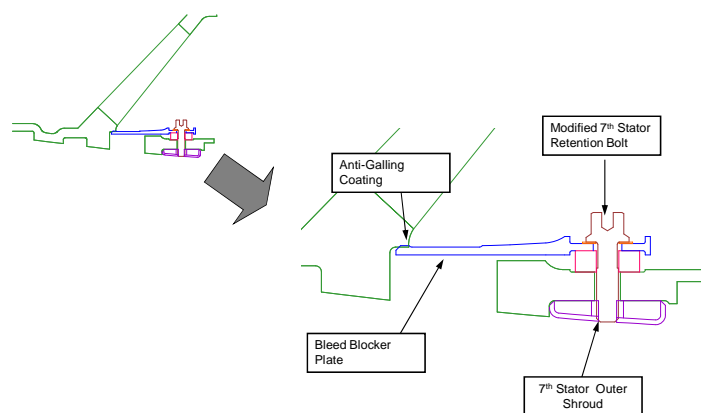


Figure 23 ETF40B 6th Bleed Production Modification

10 Conclusion

Metallographic analysis of the airfoil fracture surfaces showed fatigue striations emanating from two fracture origins. The primary fracture location was determined to be subsurface on the pressure side of the airfoil. The suction side initially was determined to be secondary to the pressure surface. This lead the root cause

investigation towards a high deflection/stress and bending fracture mode.

Finite Element Analysis (FEA) modeling of the 6th blade was successful at identifying a combined high loading condition at the primary failure location caused by high static and cyclic stresses.

Baseline engine stress map testing was accomplished with the incorporation of a light probe measurement system. This light probe system provided continuous monitoring of each blade tip deflection throughout testing. This testing proved instrumental at identifying high 4E 1st bending stresses in the 6th stage blade. These stresses were measured with the surge valve open and were 114% of the Goodman Allowable. Measured 4E 1st bending stresses were acceptable during operation with the surge valve closed during the 4E resonant crossing.

Corrective action analysis included FEA modeling and detailed Fourier analysis to aid in identifying the source of the high 4E response. The Fourier analysis proved to be instrumental at identifying hardware modifications to be incorporated into the baseline configuration. This analysis identified several configurations that were evaluated during validation testing. It also identified the 4E driver and aided in the development of a retrofitable modification to the bleed ports to remedy the issue.

Engine testing validated the concept of installing blocker plates in the bleed ports of the compressor case, modifying the forcing function on the 6th blade and reducing the resonant stresses to acceptable levels. Multiple plate configurations were evaluated; the final configuration provided the most optimized resonant stresses on the blade.

The blocker plate design was based on configuration 1, with plates installed at 45 degrees from each other creating an out of phase 4E. The plates at the MP1, MP3 and MP4 locations were 7.5 degrees wide, while the blocker plate at the MP2 location provided 50% blockage in the flow area. The design used the

7th stage stator retention bolts as a plate retaining feature.

Back to back performance testing was performed with and without the blocker plates installed in the compressor cases. The results showed no discernable difference in the performance and operability of the engine during testing.

Field retrofit of the blocker plates is in progress. Incorporation of the blocker plates is performed once the split cases are removed from the engine. Modification of the production design has been completed. These design features will be included in the split case machining and are ready for follow on production orders.